Author's Accepted Manuscript

www.elsevier.com/locate/ijadhadh

Solvent Presence and its Impact on the Lap-Shear Strength of SDS-Decorated Graphene Hybrid Electrically Conductive Adhesives

Josh Trinidad, Li Chen, Angela Lian, Boxin Zhao

PII: S0143-7496(17)30114-8
DOI: http://dx.doi.org/10.1016/j.ijadhadh.2017.06.012
Reference: JAAD2025

To appear in: *International Journal of Adhesion and Adhesives*

Received date: 16 November 2016
Accepted date: 1 May 2017

Cite this article as: Josh Trinidad, Li Chen, Angela Lian and Boxin Zhao, Solven Presence and its Impact on the Lap-Shear Strength of SDS-Decorated Graphen Hybrid Electrically Conductive Adhesives, *International Journal of Adhesio and Adhesives,* http://dx.doi.org/10.1016/j.ijadhadh.2017.06.012

Solvent Presence and its Impact on the Lap-Shear Strength of SDS-Decorated Graphene Hybrid Electrically Conductive Adhesives

Josh Trinidad[a,b,c] , Li Chen[a,b,c], Angela Lian[a], Boxin Zhao[a,b,c]*

[a]Department of Chemical Engineering, University of Waterloo, 200 University Avenue West, Waterloo ON, N2L 3G1, Canada
[b]Waterloo Institute of Nanotechnology, University of Waterloo, 200 University Avenue West, Waterloo ON, N2L 3G1, Canada
[c]Institute for Polymer Research, University of Waterloo, 200 University Avenue West, Waterloo ON, N2L 3G1, Canada

[*]Corresponding Author, Phone: 519-8884567; Department of Chemical Engineering, University of Waterloo, 200 University Avenue West, Waterloo ON, N2L 3G1, Canada . zhaob@uwaterloo.ca

Abstract

The mechanical bonding strength of electrically conductive adhesives (ECAs), as well as the impact of residual solvent on the bonding strength was investigated between a copper clad FR-4 surface and conductive adhesives using Lap-shear testing. Both solvent-free and solvent-assisted formulations with various filler concentrations of silver (Ag) and sodium dodecyl sulfate (SDS)-decorated graphene (Gr(s)) in epoxy matrices were prepared and compared. It was found that the introduction of 0.75 wt% Gr(s) in solvent-free formulations increased the Lap-shear strength (LSS), while the combination of ethanol solvent and SDS in solvent-assisted formulations significantly decreased the LSS. In addition, it was found that increasing the Ag content generally lowers the LSS for both the solvent-free and solvent-assisted formulations. By examining the structure and interface of both formulations using optical microscopy, surface profilometry and SEM, we found that the solvent-assisted formulations exhibit more voids at the surface of the paste and more bubble formation throughout the material compared to the solvent-free formulations. Therefore, the significant drops of LSS in solvent-assisted Gr(s)-filled formulations may be attributed to the formation of bubbles at the micron range during the curing process.

Keywords: Lap-shear strength, solvent, surfactant-decorated graphene, conductive adhesives

1. Introduction

In recent years, adhesives have been finding more applications owing to numerous advantages including the ability to bond two irregularly shaped surfaces, the ability to resist corrosion, efficient mechanical load transfer, and the capability to resist stress and mechanical vibrations [1–3]. Currently, the industry has been increasing the demand for high performance adhesive joint technology, as we continue to devise new applications (e.g. rotating engines for wind turbines, electronic assembly and packaging, coatings, thin-films, aerospace and automotive technology, medical device manufacturing, optics & photonics, composite materials, paints etc.) [1–5]. These adhesives can be used either as a film, coating, or as an adhesive joint [2]. For most of these applications, it is of great importance that researchers develop reliable methods to predict the performance of adhesives. However, the quantifiable prediction of the performance and the bond strength of adhesives is challenging and complex to obtain without using simulations and modeling software, because multiple factors (e.g. geometric complexity, inherent discontinuity signature between the adhesive and the surface, the failure mechanisms happening in the microscopic level) need to be accounted for [3,6]. Generally, it is beneficial to simplify the evaluation method in order to provide information that is useful and applicable to both industry and research. One strategy is to utilize well-accepted standard tests such as ASTM standards [7]. In both research labs and industrial technical datasheets, a tensile-based Lap-shear testing technique is the most common and widely used technique for determining the bonding strength and benchmarking the performance of their materials (using ASTM D1002 or equivalent). In specific, this method is extensively used for the evaluation of bonding strength between adhesives and metallic substrates [1,3,5,6,8–17].

Electrically conductive adhesives (ECAs) are adhesive composites that are primarily comprised of two materials: (a) a polymeric binder resin (typically in the form of a

thermoset (e.g. epoxy)); (b) conductive filler material (typically Ag flakes). This composite material is known as an alternative electronic packaging material to the lead-based solder, possessing desirable properties such as high shear strength, low temperature requirements, fewer processing steps, finer pitch capabilities and environmental friendliness [18]. Researchers have dedicated time and effort towards examining the properties of ECAs such as electrical/thermal conductivity, mechanical strength, thermal/mechanical/environmental reliability, and processing temperature [18,19]. However, among these properties, the electrical conductivity and mechanical strength of the conductive adhesive are of primary concern [9,18,20–22]. While most research focuses on improving the electrical conductivity of ECAs [23–27], there are limited studies on the evaluation of their mechanical properties [22]. This work aims to study the mechanical bonding properties of isotropic conductive adhesives for microelectronic packaging applications that seek to bind electrical components onto a printed circuit board (PCB).

In a recent work, we have demonstrated that sodium dodecyl sulfate (SDS)-modified graphene (Gr(s)) as a co-filler for conventional conductive adhesives (CCA) significantly improved the electrical conductivity. Graphene nanosheets are exfoliated in a non-covalent manner by SDS molecules in solvent after undergoing ultrasonic bath, thereby taking full advantage of the remarkable intrinsic properties of graphene (see [23] for details). Despite the benefits of better dispersion that solvent assistance offers, there is always a concern that thermal and mechanical properties might be negatively affected when residual solvent is present in the mixture [12,23,28]. Hence, we have employed a solvent-free method of preparing hybrid ECA composites, where the exclusion of solvent is crucial to the investigation of rheological properties [29]. The Gr(s)-filled CCAs that were prepared using the newly developed solvent-free method resulted in an increase in bulk resistance when compared to that obtained by the solvent-assisted predecessor [29]. Although it is confirmed the utilization of solvent is integral for effectively dispersing Gr(s) within the composite [23,29], the possible negative impact of presence of solvent within the system on the mechanical properties of the cured adhesive was not clarified, especially if the solvent functional groups unfavorably interact with either the polymer matrix or the surfactant [12,30–32].

In this work, we concentrate on using Lap-shear testing based on the most common test standard: ASTM D1002 [1,7] to investigate the impact of residual solvent on the bonding strength between a copper clad FR-4 surface and our hybrid ECAs. We firstly studied the mechanical bonding property of both hybrid and conventional ECAs, and then compared the mechanical bonding properties of the solvent-free formulations with those of the solvent-assisted formations. Furthermore, potential factors directly impacting the mechanical strength were investigated to gain a better understanding on the post-cured process. Finally, we seek to identify an optimal composition that possesses both high shear strength and electrical conductivity, as this result can be useful for further investigation.

2. Materials and Methods

2.1. Materials

The polymer matrix used in this study was the liquid epoxy resin (D.E.R 331™) Diglycidyl Ether Bisphenol-A (DGEBA) and amine-based curing agent triethylenetetraamine (TETA), both purchased and used as received from DOW Chemical Company (USA). Ag flakes (~10 μm) purchased from Sigma Aldrich were used as received, and acted as the conductive filler for the composite. Graphene nanosheets with a size ranging from 0.5 to 5 μm were purchased from ACS Materials (USA) and were used as received [23,29]. The surfactant SDS was purchased from Sigma Aldrich and used as received to exfoliate the graphene nanosheets. HPLC ethanol solvent at 99.8% purity was purchased and used as received from Fisher Scientific (USA).

2.2. Preparation of ECA composites

The process for preparing the composites included the following steps: (a) adding the appropriate amounts of epoxy resin and Ag flakes according to the desired composition as denoted in Table 1 (Note: all calculations are based on 120 mg of resin); (b) adding Gr(s) that was prepared by the following procedure: SDS and graphene were suspended in ultra pure water, and then, an ultra sonic bath was used to allow the surfactant to self-assemble onto the graphene sheets, and finally, the extraction of the Gr(s) by centrifugation and evaporation of any remaining supernatant [29]; (c) we conducted steps

for preparing solvent-assisted formulations, which include adding 250 μL HPLC ethanol, running the mixture through a planetary shear mixer (PSM) at 2000 RPM (mixing mode) for five minutes, and then doing a combination of two-minute vortex mixing and five-minute desiccation [23,29]; (d) adding the curing agent TETA and mixing the composite via PSM to form the ECA paste [23,29] and then applying the paste onto the appropriate test coupons (i.e. FR-4/electrical/microscopy). (e) Placing the test coupons containing the paste into an oven at 60°C for one hour. Afterwards, the oven is ramped to 150°C for two hours, allowing the ECAs to fully cure. A schematic in Fig. 1 illustrates the above method.

Table 1 List of the combinations of compositions used for nanocomposites and curing conditions.

Composition	Ag flakes (wt %)	Gr(s) (wt %)	Curing Conditions
Epoxy + Ag	20, 40, 60	0	60°C for 1 hr and then150°C for 2 hrs
Epoxy + Ag + solvent	20, 40, 60	0	60°C for 1 hr and then150°C for 2 hrs
Epoxy + Ag + Gr(s)	20, 40, 60	0.75, 1.5	60°C for 1 hr and then150°C for 2 hrs
Epoxy + Ag + Gr(s) + solvent	20, 40, 60	0.75, 1.5	60°C for 1 hr and then150°C for 2 hrs

2.3. Characterization of ECAs

2.3.1. Lap-Shear Test

The Universal Material Tester (UMT) Tribological Test Equipment (CETR Campbell), equipped with a pair of tensile wedge grips (G1061-2, Mark-10 Corp) was used to evaluate the Lap-shear strength (LSS) of varying ECA compositions (each composition was tested twice for a total of two repetitions). Test coupons (1/16" double-sided FR-4 boards, 590-540) were purchased and used as received from MG Chemicals. The specifications of the FR-4 boards were machined to follow the dimensions presented in Fig. 2. The test procedure and calculations followed ASTM D1002 [33] with the exception of reducing the contact area of the joint to 12.7 mm x 12.7 mm in order to accommodate for the limitations of the load cell used in the experiment.

2.3.2. Optical Microscopy and Surface Profilometry

The bonding interfaces of two ECA formulations were observed under manual operation using an inverted optical microscope (Carl Zeiss Axio Observer Z1m;

Magnification 5x and 50x) equipped with a CCD camera (Axio Cam 1Cm1). The sample paste (as denoted in Fig. 2c) was casted onto a 12.7 mm x 12.7 mm mold similar to the Lap-shear coupons. However, instead of using FR-4 boards, standard soda-lime microscope glass slides purchased from Fisher Scientific (cat #: 12-544-1) were used instead (as received), taking advantage of glass transparency, as well as the opaqueness of the paste and its reflective properties as the light shines through the glass to characterize the hybrid ECA.

An optical profilometer (MFP-D WLI 3D Surface Profilometer, RTEC Instruments USA) based on the light interference was used to observe the surface roughness of the solvent-assisted and solvent-free ECAs (after the LSS testing) and was used to generate a 3D plot to further illustrate the difference in contact area, as well as any other paste defects that are not easily detectable by optical imaging.

2.3.3. Scanning Electron Microscopy

A Field Emission Scanning Electron Microscope (FE-SEM, LEO-Ultra, Gemini, Germany) was used in order to investigate the morphology, and if possible, find potential defects or bubbles associated with the solvent-assisted method. ECA pastes were casted onto a mold prepared by placing thermally resistant tape onto a 12.7 mm x 12.7 mm area on glass slides, and a thin sheet of copper was used as a cover for the ECA. The glass slide was then sliced and bent (at the middle of the copper sheet) in order to obtain a flattened cross-sectional sample of the ECA. The samples were placed on a 90-degree stub to view the cross-section of the ECA.

2.4. Electrical Conductivity Test

A four-point probe fixture (Cascade Microtech Inc.) that is connected to a micro-ohm meter (Keithley 2440 5A Source Meter, Keithley Instruments Inc.) was used to measure the electrical sheet-resistance of ECAs. These values were then converted to bulk resistance ρ using the following equations [25,34]:

$$\rho = R_s \cdot t = F \cdot t \left(\frac{\pi}{\ln 2}\right) \frac{V}{I} \quad (1)$$

The sheet resistance (R_s) obtained from the reading was used together with the caliper-measured ECA thickness (t). The (I) and (V) represent the applied current and measured

voltage drop across the probe pins, respectively. The correction factor (F) is the ratio between the thickness of the ECA sample (t) and the probe gap (s) which is the distance between each adjacent point (or prong) in the probe [25,34]. Under the condition where $0.4 < \frac{t}{s} < 1$, it is safe to approximate the correction factor (F) to equal 1 [25,34]. As the probe gap is 1 mm wide, the ECAs prepared were designed to have an average thickness of 0.5 to 0.7 mm, resulting in the fulfillment of the above stated condition.

3. Results and discussion

In order to investigate the impact of concentrations of Ag flakes and Gr(s) on the behaviors of the final hybrid ECAs, we examined the variation of LSS (in MPa) with the weight concentrations of Gr(s) and Ag. In addition, we compared the solvent-free method with the solvent-assisted method as seen in Fig. 3.

3.1. The LSS of hybrid ECAs prepared from solvent-free method

The LSS values for the solvent-free formulations with various weight concentrations of Ag and Gr(s) were shown in Fig. 3a. With the increase of Gr(s) wt% at a constant Ag wt%, we can see that the LSS has a maximum value; the LSS is at its highest for a weight loading of 0.75 wt% Gr(s) and lower values for both 0 wt% and 1.5 wt% Gr(s) (this is for all three weight concentrations of Ag). This observation is in agreement with those of the CNT-containing ICAs that were applied onto an aluminum substrate as demonstrated by H.P. Wu et al [35]. Furthermore, it is observed that the LSS value for 0.75 wt% Gr(s) has the smallest deviation among all of the formulations. Based on our results, 0.75 wt% Gr(s) successfully increased the strength of the composite. However, 1.5 wt% Gr(s) experienced a decrease in LSS, which is likely due to the aggregation of Gr(s). Zandiatashbar et al reported on the agglomeration behavior within graphene platelet composites, stating that the graphene clustered at higher concentrations, resulting in the composites of weaker mechanical properties [36]. We hypothesize that 0.75 wt% loading of Gr(s) into the composite is the highest (and optimal) loading that the system can handle before the nanoparticles favor clustering to each other, resulting in poor dispersion and weaker mechanical strength especially at the interface.

As the Ag wt% increases at a constant Gr(s) wt%, the LSS of the composite decreases. Formulations that contain 0.75 wt% Gr(s) display the smallest decline while the sharpest decline is observed for formulations that do not contain Gr(s). It is also interesting to note that the LSS deviation is consistently large for the formulations that only contain Ag. The sharp decline and large deviation suggests that increasing Ag in ECAs without Gr(s) shows increasing unreliability with large error bars and decreasing mechanical strength, which conflicts with the idea that higher weight concentrations of Ag are desirable in attaining better electrical performance [35]. This is reasonable as the increase of the Ag filler content in the composite means the decrease of epoxy (the actual binding component) relative to the total volume of the composite, resulting in the decrease of the ECAs shear strength [35]. It has been known that excess Ag content in conventional ECAs leads to issues such as higher material costs, little to no electrical conductivity improvement (past the percolation threshold), and poor environmental reliability [9,24,35,37,38]. However, this work also shows there is a detrimental effect to the LSS of our composite when using an excess amount of Ag filler content, which further supports the need to reduce the amount of Ag in conventional ECAs.

When comparing the two filler materials, it has been shown that Gr(s) has the potential to act as a reinforcing agent upon reaching a critical concentration. Moreover, there is little variance among the samples, resulting in a mechanically reliable and robust ECA. On the other hand, this work specifically shows that excess addition of the Ag flakes into our electrically conductive composite is detrimental to its mechanical strength and should be avoided to prevent introducing weakness, cost and any negative impact to the environmental reliability of the ECA.

3.2. The LSS of hybrid ECAs prepared from solvent-assisted method

The LSS values of the solvent-assisted formulations were investigated to follow up initial suspicions (from other references and our previous work) that the presence of residual solvent in the ECA composites negatively impacted the mechanical properties [12,23]. The LSS values for the solvent-assisted formulations with various weight concentrations of Ag and Gr(s) were determined. Fig. 3b illustrates significant drops in LSS values when Gr(s) was introduced as co-fillers, and this trend was identical for all

three Ag-containing solvent-assisted formulations. It is important to note that although it is true that solvent potentially has the ability to improve the dispersion of the nanocomposite fillers, the presence of even trace amounts of solvent (despite desiccation or evaporation) can negatively impact the thermal and mechanical properties of nanocomposites (in our specific case, the mechanical bonding properties [12,23]). These results verify this negative effect: the assistance of solvent was shown to exhibit lower shear strengths, especially when compared to the solvent-free formulations (Fig. 3a).

As for formulations without Gr(s), both solvent-free formulations and solvent-assisted formulations at 20 wt% Ag concentrations share similar LSS values of ~5 MPa. However, formulations with 40 wt% Ag and 60 wt% Ag possessed LSS values of 4.2 MPa and 2.8 MPa respectively, indicating that a gradual decrease in the LSS values occurs when the Ag concentrations for the solvent-free formulations was increased. As for solvent-assisted formulations, no dramatic decrease of LSS values was observed for formulations with 40 wt% Ag (4.6 MPa) and 60 wt % Ag (~4.9 MPa). Therefore, for Gr(s)-free formulations, the presence of residual ethanol alone in the system did not disrupt the curing mechanism of the ECA, but instead enhanced the mechanical property by assisting the dispersion of Ag flakes. By comparing Fig. 3a with Fig. 3b, we could conclude that the coexistence of SDS and residual ethanol was responsible for the drop in the LSS values. To explain this drop in LSS values, we first considered the findings of our previous thermal characterization of ECAs in terms of its curing behavior. Three findings were stated that would help elucidate the results seen in Fig. 3b: (a) Ag flakes have no significant effect on the curing of epoxy [28]; (b) the presence of trace ethanol in the composite reduced both the enthalpy of the curing reaction (ΔH_{Tot}) and final glass transition value ($T_{g\infty}$), indicating a possible drop in epoxy's crosslinking density [23]. In addition, there is also the possibility of solvent evaporation happening in the sample that contains trace solvent, or perhaps dilution effects are taking place within the system as was suggested in Amoli et al's work [23], which should be investigated in future work; (c) the addition of ethanol into epoxy led to a sudden increase to the enthalpy normalized to the mass of epoxy hardener (ΔH_{norm}) as measured by DSC compared with neat epoxy, and for the hybrid ECA-containing graphene compared with the hybrid ECA containing Gr(s) [23]. Furthermore, to address the impact of surfactant SDS, Amoli et al reported

that when they compared the hybrid ECAs containing Gr(s) to the one without SDS, no significant change in $T_{g\infty}$ was observed; instead, a reduction in ΔH_{norm} was seen, which points to an unknown mechanism that is caused by the presence of SDS [23]. One hypothesis points to the possibility that SDS and ethanol are competing with the main stoichiometric chemistry of the epoxy, which as a result, changes the thermal data and crosslinking density of the final product [23]. Although the mechanism itself was not confirmed, findings in this work appear to support the initial suspicions outlined in previous work, since the presence of both solvent and surfactant negatively impact the mechanical bonding properties of the cured adhesive. Further work using thermal characterization techniques and direct measurement of the bulk mechanical properties of ECAs are recommended to examine the interaction of solvent with surfactant negatively affects the crosslinking density.

Overall, it is evident that the strongest solvent-free formulations are those that contain 0.75 wt% Gr(s). Among these, 0.75 wt% Gr(s) with 60 wt% Ag and 0.75 wt% Gr(s) with 40 wt% Ag will be further tested by microscopy techniques and for electrical conductivity. The reason why the highest LSS value in the solvent-free process (20 wt% Ag and 0.75 wt% Gr(s)) was not chosen for further testing comes from the fact that formulations with low Ag content (20 wt%) express little to no electrical conductivity, thereby eliminating its potential to be used as a functioning ECA.

Another factor that was suspected to contribute to the decrease in mechanical bonding strength of the solvent-assisted mechanism would be the formation of bubbles during the curing process. The presence of bubbles leads to a decrease in the smoothness of the paste, as well as the contact area between the adhesive and substrate. If the paste is not smooth on the microscopic level, the actual contact area of the adhesive is reduced, thereby causing the adhesive to fail at lower applied forces.

3.3. The morphology and structure difference between solvent-free and solvent-assisted formulations

In order to verify whether or not residual solvent affects the interface, we chose to use glass with high transparency as the alternate substrate so that optical microscopy and optical profilometry techniques could be used to inspect the surface of both the solvent-

free and solvent-assisted formulations. Other factors besides substrate choice (for example, applied pressure and curing time/temperature) were kept constant. The goal of this investigation was to search for any evidence of bubbling at the interface or cross-section of the paste. Optical microscopy was used to qualitatively check for voids or other forms of discontinuity when adhering to the surface of the glass, while the optical profiler was used to generate a 3D plot to show how much of the paste is making contact with the substrate using a quantitative measure of the sample's "nominal roughness". Furthermore, the cross-section of the paste was examined using SEM to determine whether or not bubble formation was happening throughout the bulk of the composite or if it was limited to the interface between the ECA paste and the substrate.

3.3.1. Optical microscopy

The first method used to characterize the surface between the substrate and paste was the optical microscope. Both solvent-free and solvent-assisted 60 wt% Ag/0.75 wt% Gr(s) formulations were observed at 5x and 50x magnifications. Fig. 4 shows the images for solvent-free (4a) and solvent-assisted (4b) formulations under low magnification, and solvent-free (4c) and solvent-assisted (4d) formulations under high magnification.

Fig. 4a shows a speckled pattern that contains large light speckles and overall higher particle density; Fig. 4b shows smaller light speckles but in more clumps indicating that some form of aggregation may be occurring or that certain spots have more adhesion to the substrate than others. However, this still hints that the contact area between the substrate and paste for solvent-assisted formulations is smaller compared to the solvent-free formulations. This is evident in the higher magnification images in Fig. 4c and 4d, as there are more clumps visible for the solvent-assisted formulations. In order to perceive the clumps, it is best to examine how large the area is for each white speckle in Fig. 4c and 4d. These white speckles represent spots that are in direct contact with the glass slide, whereas the dark spots (or voids) represent areas that are not in contact with the surface of the glass slide. The biggest observation to take from these images is that there are much larger areas that are primarily dark (these areas are voids), indicating that the real bonded area at the interface is low. This is because only some spots on the sample (the ones that are primarily light) are well adhered to the glass slide interface.

This observation is contrary to Fig. 4a and 4c where the distribution is more even and free of large dark spots. Similar results were also found for the 40 wt% Ag/0.75 wt% Gr(s) formulations, where more clumps were observed for the solvent-assisted formulation (Fig. S1).

These qualitative findings support the idea that the solvent-assisted formulations are indeed forming more bubbles post-cure as opposed to the solvent-free formulations. The solvent-free formulations tend to exhibit better smoothness and uniformity, which results in a joint that possesses a higher contact area between the paste and substrate, and thus higher LSS. However, a more quantitative approach is required in order to verify these observations.

3.3.2. Optical profilometry

An optical profilometer was used in order to quantitatively determine the "nominal roughness" of the paste. This technique intended to find any voids caused by the formation of bubbles during the curing by quantitatively examining how much of the paste is in contact with the glass. All samples were observed at a magnification of 10x (i.e. a scanning area of 4.435 mm x 3.548 mm), and the surface roughness values were determined and summarized in Table 2.

The paste surface from the FR-4 boards after completing the LSS tests were first analyzed. The data for 40 wt% Ag/0.75 wt% Gr(s) (Fig. S2), as well as 60 wt% Ag/0.75 wt% Gr(s) (Fig. S3) show elevation differences and what appears to be a valley-like surface, likely caused by either the applied shear force during the mechanical test, or from partial cohesive failure. Therefore, these results do not represent the real interface we are interested in investigating. Instead, we used the optical profilometer as a tool to investigate the interface's profile between a glass substrate and the paste using the test coupon in Fig. 2c. The advantage of this method is that we can aim the light probe to go further than the thickness of the glass sheet to investigate the degree of contact our paste has on a substrate, verifying whether or not there are voids at the interface. It is important to note that our surface roughness measurements can no longer be considered a true measure of surface roughness. As such, we call it a "nominal roughness" as these

numerical values no longer describe surface roughness, but instead the degree of contact our paste has on the glass substrate.

As a control experiment, the surface of a bare glass substrate was analyzed first (Fig. S4), and the images were observed to have a smooth surface with an average roughness (Ra) of 0.03 μm and a root-mean square roughness (Rms) of 0.08 μm. Similar to the optical microscope, both solvent-free and solvent-assisted formulations were compared. Both formulations with 60 wt% Ag/0.75 wt% Gr(s) (Fig. 5) and 40 wt% Ag/0.75 wt% Gr(s) (Fig. S5) were studied. Fig. 5a and 5b show the optical profile of the solvent-free paste to glass interface and the 3D render of the interface, while Fig. 5c and 5d show the optical profile of the solvent-assisted paste to glass interface and the 3D render of the interface. It was found that the solvent-free formulations exhibited a lower Ra of 3.68 μm and Rms of 4.52 μm when compared to the solvent-assisted formulations with a Ra of 3.77 μm and a Rms of 4.65 μm. The difference can be seen visually through the interface diagrams of 60 wt% Ag/0.75 wt% Gr(s) composites in Fig. 5a and 5c; Fig. 5a contains fewer dark blue areas compared to Fig. 5c. Furthermore, by looking at the 3D render of the interfaces, we notice that the solvent-assisted formulation in Fig. 5b has fewer voids when compared to the solvent-free formulation in Fig. 5d, suggesting that solvent-assisted paste had less contact with the substrate, making this surface more prone to failing at lower applied forces [39].

As for formulations of 40 wt% Ag/0.75 wt% Gr(s), the difference between solvent-free and solvent-assisted formulations was more obvious. While the optical profile results show no deep blue areas for the solvent-free formulation and a low Ra of 0.59 μm, the solvent-assisted formulation was seen with dark blue voids throughout the glass/paste interface with a Ra of 5.27 μm. After comparing the solvent-free and solvent-assisted interfaces, we found that the solvent-free formulations were smoother and contained less voids when compared to the solvent-assisted formula, supporting the idea that bubbles forming during curing decreases the contact area between the paste and substrate (which as a result, weakens the composite LSS).

Table 2 Summary of surface roughness values from optical profiler

Formulation	Ra (μm)	Rms (μm)
Standard Soda-lime Microscope Glass Slide	0.03	0.08
40 wt% Ag/0.75 wt% Gr(s) solvent-free	0.59	1.27
40 wt% Ag/0.75 wt% Gr(s) solvent-assisted	5.27	6.48
60 wt% Ag/0.75 wt% Gr(s) solvent-free	3.68	4.52
60 wt% Ag/0.75 wt% Gr(s) solvent-assisted	3.77	4.65

3.3.3. Scanning electron microscopy

In order to further verify these results, a scanning electron microscope was used to examine the cross-section of the paste at the micron range for the 60 wt% Ag/0.75 wt% Gr(s) formulations (Fig. 6). Fig. 6a and Fig. 6b denote the cross-section of solvent-free formulations under different magnifications. Fig. 6c and Fig. 6d show the cross-section of solvent-assisted formulations. Orange boxes in Fig. 6a and Fig. 6c correspond to the areas where images with higher magnifications were taken. The cross-sections of the solvent-assisted and non-solvent methods were compared. The images obtained from the SEM agree with the observations obtained from the optical microscope and optical profilometer, as the solvent-free method exhibits a smoother morphology and fewer voids or pockets (Fig. 6a and Fig. 6c) when compared to the solvent-assisted method (Fig. 6b and Fig. 6d). However, since the SEM images are able to capture interior structure of the bulk material, it is clear that the phenomenon that was observed at the surface extends throughout the entire cross section, meaning that the bubbles are not limited to the surface alone, but extends throughout the entire paste. Similar structure differences in the cross-section were also observed for formulations with 40 wt% Ag/0.75 wt% Gr(s) (Fig. S6). As such, the detrimental effects of having residual solvent within the composite can be attributed to the formation of voids and hollow structures both within the composite, as well as between the substrate/paste interface. This bubble formation that originates from residual solvent therefore weakens the mechanical bonding properties of ECAs at the interface between the FR-4 board and the paste [39].

3.4. Electrical conductivity of composites

Considering the importance of conductivity for ECAs, we also investigated the impact of solvent on conductivity for the following formulations: 40 wt% Ag/0.75 wt%

Gr(s) and 60 wt% Ag/0.75 wt% Gr(s). The presence of solvent matters for the 40 wt% Ag/0.75 wt% Gr(s) formulation, as the solvent-assisted method is observed to have bulk resistivity that is 18x smaller than the solvent-free method. However, the higher Ag content formulations (60 wt% Ag/0.75 wt%) exhibit roughly the same bulk resistivity values of $1 \times 10^{-2}\ \Omega \cdot cm$ without regard to being solvent-free or solvent-assisted. Moreover, the above electrical conductivity values are found to be congruent with Trinidad et al's findings [29]. On the other hand, when it came to Amoli et al's findings using their own solvent-assisted method, the electrical conductivities found in this work were lower by a factor of 10 [23]. This is likely because the procedure in this work dispersed the filler in the epoxy first, which in effect differs from Amoli et al's procedure where filler content was added to solvent first and then dispersed with epoxy. This difference might result i better dispersion and better electrical conductivities n their formulation. Further work is required to verify this. Overall, the chosen solvent-free composites exhibited conductivity values that are considered acceptable for electrically conductive adhesives, while also showing high LSS values. These findings conclude that 60 wt% Ag/0.75 wt% Gr(s) formulation is the optimal formulation for high LSS and high conductivity, while retaining a relatively simple preparation method when compared to the solvent-assisted approach.

4. Conclusions

In this work, the LSS of both solvent-free and solvent-assisted formulations filled with various concentrations of Ag flakes and Gr(s) were studied. For solvent-free formulations, the addition of 0.75 wt% Gr(s) increased the LSS, while any further increase of Gr(s) showed a negative impact on the LSS. For solvent-assisted formulations, the combination of solvent presence and Gr(s) within the composite showed a dramatic decrease in the LSS of the hybrid ECAs, while high LSS values were achieved for hybrid ECAs without Gr(s) under all Ag concentrations. In both cases, the increase of Ag concentrations in formulations resulted in a decrease in the LSS. By using the optical microscopy and optical profilometer, we found that the solvent-assisted formulations exhibited more voids and a smaller contact area at the bonding interface when compared to the solvent-free formulations (which as a result weakens the

mechanical bonding properties of the ECA). In addition, the SEM analyses of the cross-section further confirmed that bubble formation occurred throughout the material rather than being confined to the interface. This resulting structural difference between the solvent-free and solvent-assisted formulations indicates that the large drop in LSS in the Gr(s)-filled solvent-assisted formulations was attributed to the formation of bubbles at the micron range during the curing process. As for conductivity, solvent-assisted ECAs with Ag 40 wt% Ag showed significantly lower bulk resistivity than its solvent-free counterpart, whereas solvent-assisted and solvent-free formulations with 60 wt% Ag exhibited roughly the same bulk resistivity. Therefore, ECA with 60 wt% Ag/0.75 wt% Gr(s) exhibited the best electrical and mechanical properties.

5. Acknowledgements

The authors want to thank the Refined Manufacturing Acceleration Process Network (ReMAP), Natural Sciences and Engineering Research Council of Canada (NSERC) for their financial support on this project.

References

[1] Quispe Rodríguez R, de Paiva WP, Sollero P, Bertoni Rodrigues MR, de Albuquerque ÉL. Failure criteria for adhesively bonded joints. Int J Adhes Adhes 2012;37:26–36. doi:10.1016/j.ijadhadh.2012.01.009.

[2] Yacobi BG, Martin S, Davis K, Hudson A, Hubert M. Adhesive bonding in microelectronics and photonics. J Appl Phys 2002;91:6227. doi:10.1063/1.1467950.

[3] HATTORI T. A stress-singularity-parameter approach for evaluating adhesive strength of single joints. Trans Japan Soc Mech Eng Ser A 1990;56:618–23. doi:10.1299/kikaia.56.618.

[4] Belnoue JP-H, Giannis S, Dawson M, Hallett SR. Cohesive/adhesive failure interaction in ductile adhesive joints Part II: Quasi-static and fatigue analysis of double Lap joint specimens subjected to through-thickness compressive loading. Int J Adhes Adhes 2016;68:369–78. doi:10.1016/j.ijadhadh.2016.03.010.

[5] Khan U, May P, Porwal H, Nawaz K, Coleman JN. Improved Adhesive Strength

and Toughness of Polyvinyl Acetate Glue on Addition of Small Quantities of Graphene. ACS Appl Mater Interfaces 2013;5:1423–8. doi:10.1021/am302864f.

[6] da Costa Mattos HS, Sampaio EM, Monteiro AH. Static failure analysis of axially loaded aluminium–epoxy butt joints. Int J Adhes Adhes 2010;30:774–80. doi:10.1016/j.ijadhadh.2010.08.004.

[7] Her S-C. Stress analysis of adhesively-bonded Lap joints. Compos Struct 1999;47:673–8. doi:10.1016/S0263-8223(00)00052-0.

[8] Moriche R, Prolongo SG, Sánchez M, Jiménez-Suárez A, Chamizo FJ, Ureña A. Thermal conductivity and Lap shear strength of GNP/epoxy nanocomposites adhesives. Int J Adhes Adhes 2016;68:407–10. Doi:10.1016/j.ijadhadh.2015.12.012.

[9] Zwolinski M, Hickman J, Rubin H, Zaks Y, McCarthy S, Hanlon T, et al. Electrically conductive adhesives for surface mount solder replacement. IEEE Trans Components, Packag Manuf Technol Part C 1996;19:241–50. doi:10.1109/3476.558550.

[10] de Morais AB, Pereira AB, Teixeira JP, Cavaleiro NC. Strength of epoxy adhesive-bonded stainless-steel joints. Int J Adhes Adhes 2007;27:679–86. doi:10.1016/j.ijadhadh.2007.02.002.

[11] Khoee S, Hassani N. Adhesion strength improvement of epoxy resin reinforced with nanoelastomeric copolymer. Mater Sci Eng A 2010;527:6562–7. doi:10.1016/j.msea.2010.07.013.

[12] Gupta ML, Sydlik SA, Schnorr JM, Woo DJ, Osswald S, Swager TM, et al. The effect of mixing methods on the dispersion of carbon nanotubes during the solvent-free processing of multiwalled carbon nanotube/epoxy composites. J Polym Sci Part B Polym Phys 2013;51:410–20. doi:10.1002/polb.23225.

[13] Khan NI, Halder S, Goyat MS. Effect of epoxy resin and hardener containing microcapsules on healing efficiency of epoxy adhesive based metal joints. Mater Chem Phys 2016;171:267–75. doi:10.1016/j.matchemphys.2016.01.017.

[14] Hansen N, Adams DO, DeVries KL, Goff A, Hansen G. Investigation of Electrically Conductive Structural Adhesives using Nickel Nanostrands. J Adhes Sci Technol 2011;25:2659–70. doi:10.1163/016942411X556033.

[15] Lee CY, Bae J-H, Kim T-Y, Chang S-H, Kim SY. Using silane-functionalized graphene oxides for enhancing the interfacial bonding strength of carbon/epoxy composites. Compos Part A Appl Sci Manuf 2015;75:11–7. doi:10.1016/j.compositesa.2015.04.013.

[16] Zhai LL, Ling GP, Wang YW. Effect of nano-Al2O3 on adhesion strength of epoxy adhesive and steel. Int J Adhes Adhes 2008;28:23–8. doi:10.1016/j.ijadhadh.2007.03.005.

[17] Sydlik SA, Lee J-H, Walish JJ, Thomas EL, Swager TM. Epoxy functionalized multi-walled carbon nanotubes for improved adhesives. Carbon N Y 2013;59:109–20. doi:10.1016/j.carbon.2013.02.061.

[18] Li Y, Wong CP. Recent advances of conductive adhesives as a lead-free alternative in electronic packaging: Materials, processing, reliability and applications. Mater Sci Eng R Reports 2006;51:1–35. doi:10.1016/j.mser.2006.01.001.

[19] Tan F, Qiao X, Chen J, Wang H. Effects of coupling agents on the properties of epoxy-based electrically conductive adhesives. Int J Adhes Adhes 2006;26:406–13. doi:10.1016/j.ijadhadh.2005.06.005.

[20] Siau S, Vervaet A, Schacht E, Van Calster A. Influence of Chemical Pretreatment of Epoxy Polymers on the Adhesion Strength of Electrochemically Deposited Cu for Use in Electronic Interconnections. J Electrochem Soc 2004;151:C133. doi:10.1149/1.1639159.

[21] Guan Y, Chen X, Li F, Gao H. Study on the curing process and shearing tests of die attachment by Ag-epoxy electrically conductive adhesive. Int J Adhes Adhes 2010;30:80–8. doi:10.1016/j.ijadhadh.2009.09.003.

[22] Uddin MA, Alam MO, Chan YC, Chan HP. Adhesion strength and contact resistance of flip chip on flex packages—effect of curing degree of anisotropic conductive film. Microelectron Reliab 2004;44:505–14. doi:10.1016/S0026-2714(03)00185-9.

[23] Meschi Amoli B, Trinidad J, Rivers G, Sy S, Russo P, Yu A, et al. SDS-stabilized graphene nanosheets for highly electrically conductive adhesives. Carbon N Y 2015;91:188–99. doi:10.1016/j.carbon.2015.04.039.

[24] Amoli BM, Marzbanrad E, Hu A, Zhou YN, Zhao B. Electrical Conductive Adhesives Enhanced with High-Aspect-Ratio Silver Nanobelts. Macromol Mater Eng 2014;299:739–47. doi:10.1002/mame.201300295.

[25] Meschi Amoli B, Trinidad J, Hu A, Zhou YN, Zhao B. Highly electrically conductive adhesives using silver nanoparticle (Ag NP)-decorated graphene: the effect of NPs sintering on the electrical conductivity improvement. J Mater Sci Mater Electron 2015;26:590–600. doi:10.1007/s10854-014-2440-y.

[26] Jiang H, Moon K, Li Y, Wong CP. Surface Functionalized Silver Nanoparticles for Ultrahigh Conductive Polymer Composites. Chem Mater 2006;18:2969–73. doi:10.1021/cm0527773.

[27] Jeong W-J, Nishikawa H, Itou D, Takemoto T. Electrical Characteristics of a New Class of Conductive Adhesive. Mater Trans 2005;46:2276–81. doi:10.2320/matertrans.46.2276.

[28] Rivers G, Rogalsky A, Lee-Sullivan P, Zhao B. Thermal analysis of epoxy-based nanocomposites: Have solvent effects been overlooked? J Therm Anal Calorim 2015;119:797–805. doi:10.1007/s10973-013-3613-2.

[29] Trinidad J, Amoli BM, Zhang W, Pal R, Zhao B. Effect of SDS decoration of graphene on the rheological and electrical properties of graphene-filled epoxy/Ag composites. J Mater Sci Mater Electron 2016. doi:10.1007/s10854-016-5434-0.

[30] Khan U, Ryan K, Blau WJ, Coleman JN. The effect of solvent choice on the mechanical properties of carbon nanotube–polymer composites. Compos Sci Technol 2007;67:3158–67. doi:10.1016/j.compscitech.2007.04.015.

[31] Coleman JN, Khan U, Blau WJ, Gun'ko YK. Small but strong: A review of the mechanical properties of carbon nanotube–polymer composites. Carbon N Y 2006;44:1624–52. doi:10.1016/j.carbon.2006.02.038.

[32] Lau K, Lu M, Cheng H, Sheng F, Li H. Thermal and mechanical properties of single-walled carbon nanotube bundle-reinforced epoxy nanocomposites: the role of solvent for nanotube dispersion. Compos Sci Technol 2005;65:719–25. doi:10.1016/j.compscitech.2004.10.005.

[33] ASTM D1002. ASTM D1002: Standard Test Method for Apparent Shear Strength of Single-Lap-Joint Adhesively Bonded Metal Specimens by Tension Loading (

Metal-to-Metal). Standards 2005:1–5.

[34] Meschi Amoli B, Hu A, Zhou NY, Zhao B. Recent progresses on hybrid micro–nano filler systems for electrically conductive adhesives (ECAs) applications. J Mater Sci Mater Electron 2015;26:4730–45. doi:10.1007/s10854-015-3016-1.

[35] Wu H, Wu X, Ge M, Zhang G, Wang Y, Jiang J. Properties investigation on isotropical conductive adhesives filled with silver coated carbon nanotubes. Compos Sci Technol 2007;67:1182–6. doi:10.1016/j.compscitech.2006.05.010.

[36] Zandiatashbar a., Picu RC, Koratkar N. Mechanical Behavior of Epoxy-Graphene Platelets Nanocomposites. J Eng Mater Technol 2012;134:31011. doi:10.1115/1.4006499.

[37] Pu N-W, Peng Y-Y, Wang P-C, Chen C-Y, Shi J-N, Liu Y-M, et al. Application of nitrogen-doped graphene nanosheets in electrically conductive adhesives. Carbon N Y 2014;67:449–56. doi:10.1016/j.carbon.2013.10.017.

[38] Daoqiang Lu, Tong QK, Wong CP. Mechanisms underlying the unstable contact resistance of conductive adhesives. IEEE Trans Electron Packag Manuf 1999;22:228–32. doi:10.1109/6104.795858.

[39] Somekawa H, Watanabe H, Mukai T, Higashi K. Low temperature diffusion bonding in a superplastic AZ31 magnesium alloy. Scr Mater 2003;48:1249–54. doi:10.1016/S1359-6462(03)00054-X.

Figures

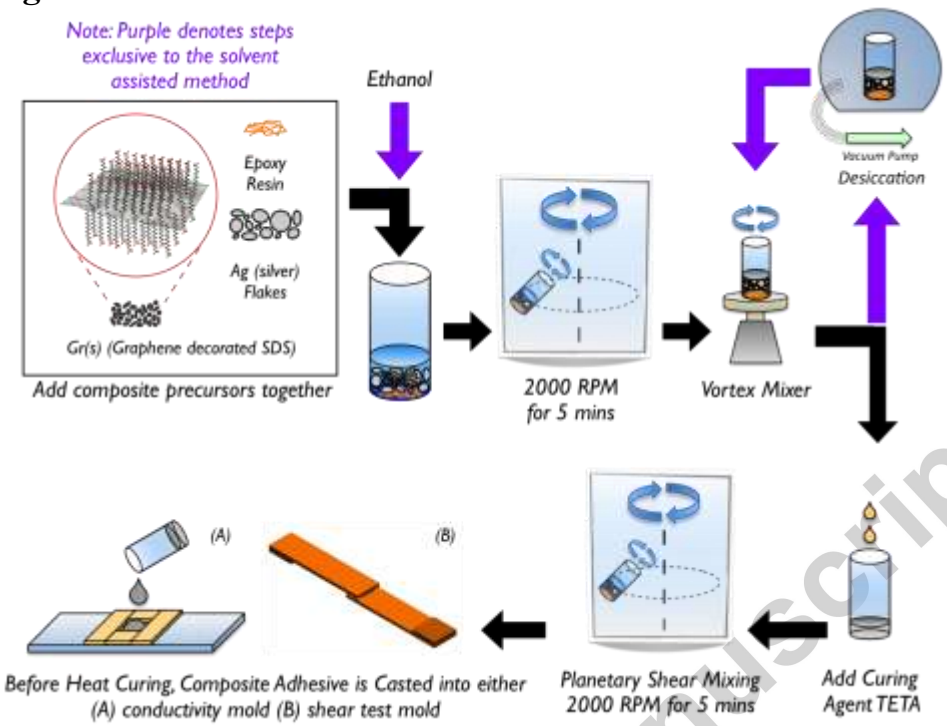

Fig. 1. A schematic illustration showing how the ECAs were mixed and prepared for testing. The precursors are all added together into a vial, which is then mixed using a planetary shear mixer. The paste is then vortex mixed and curing agent is added. After adding curing agent, the composite is again mixed in the planetary shear mixer and casted into respective test molds for characterization.

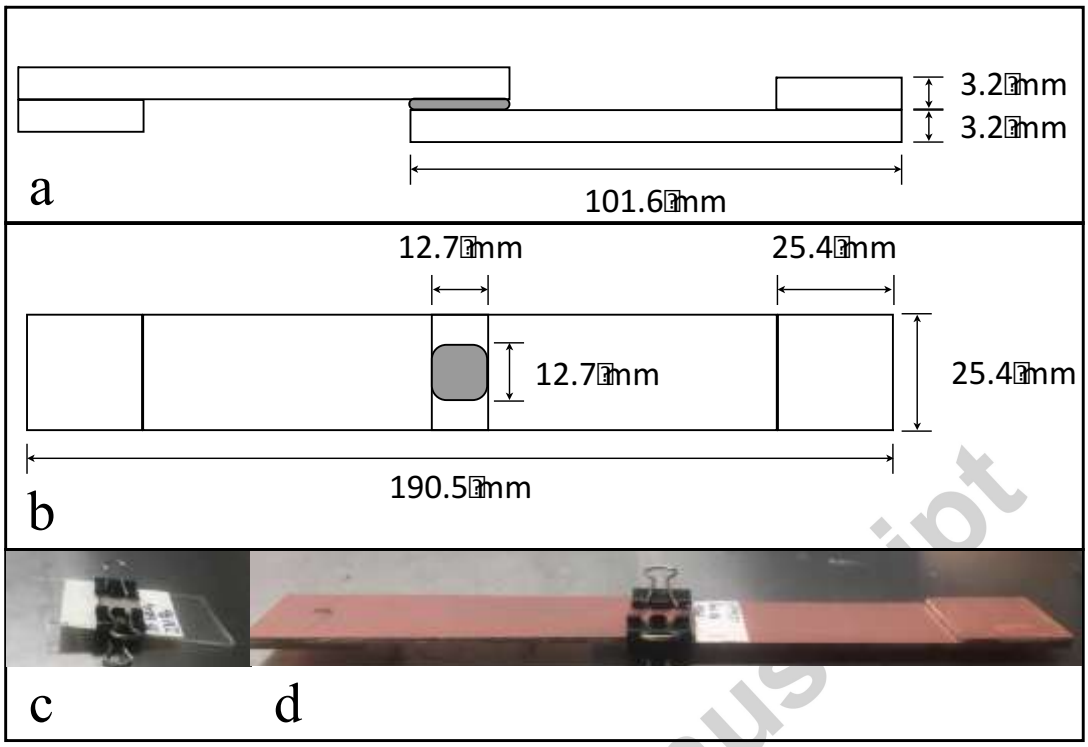

Fig. 2. A schematic showing the test coupons used. (a) Cross-section illustration of ASTM D1002 test coupon and its modified paste measurements. (b) Top view for ASTM D1002 test coupon illustration detailing its modified paste measurements. (c) Example of test coupon used for viewing surface of paste using optical microscopy and optical profiling. (d) Example of test sample used for ASTM D1002 Lap-shear testing.

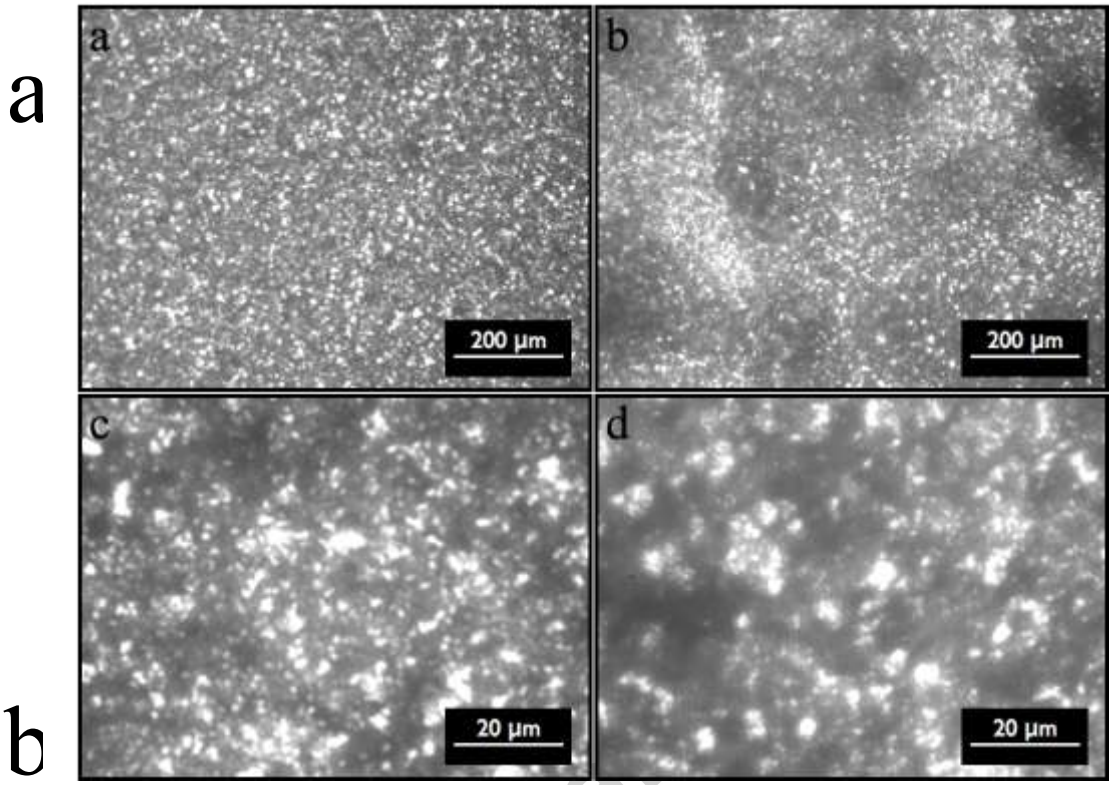

Fig. 3. The LSS bar graphs for hybrid ECAs. (a) Values of hybrid ECAs prepared with solvent-free method. (b) Values of hybrid ECAs prepared with solvent-assisted method.
Fig. 4. Optical microscopy images of hybrid ECAs with 60 wt% Ag/0.75 wt% Gr(s). (a) Solvent-free formulation at low magnification. (b) Solvent-assisted formulation at low magnification. (c); Solvent-free formulation at high magnification. (d) Solvent-assisted formulation at high magnification.

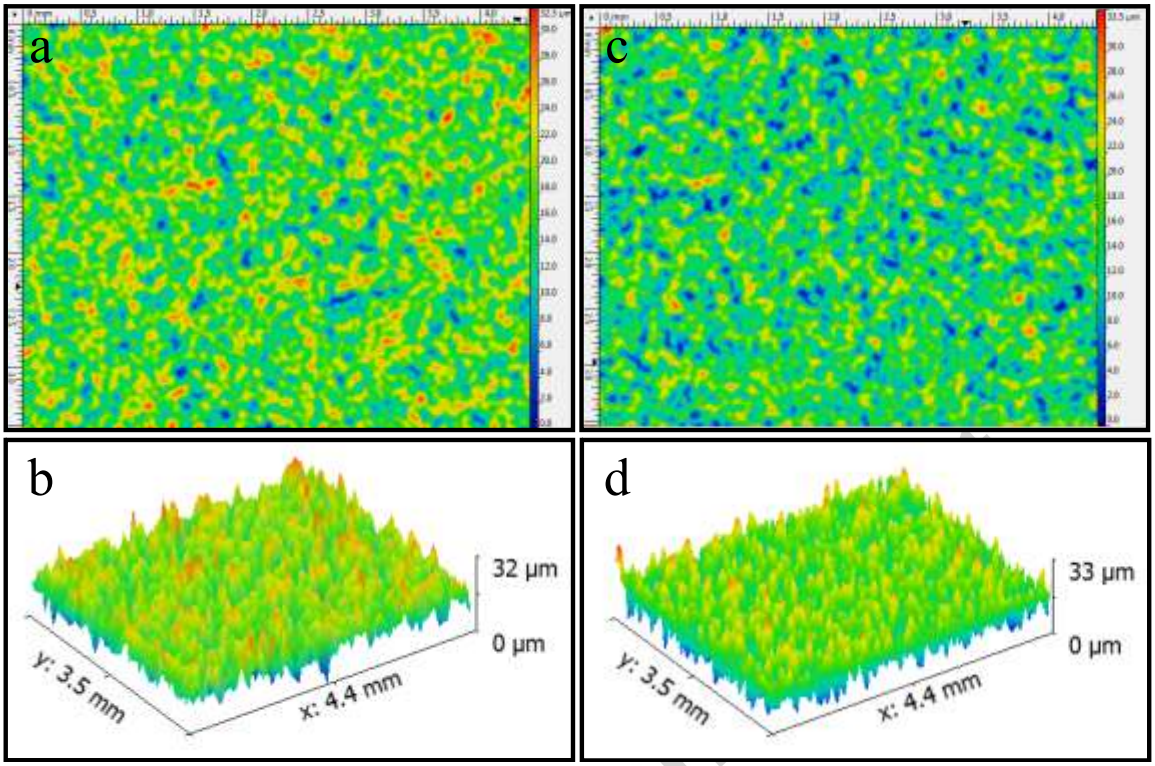

Fig. 5. Optical Profiles of hybrid ECAs with 60 wt% Ag/0.75 wt% Gr(s). (a) 2D interface profile of solvent-free formulation. (b) 3D interface profile of solvent-free formulation. (c) 2D interface profile of solvent-assisted formulation. (d) 3D interface profile of solvent-assisted formulation.

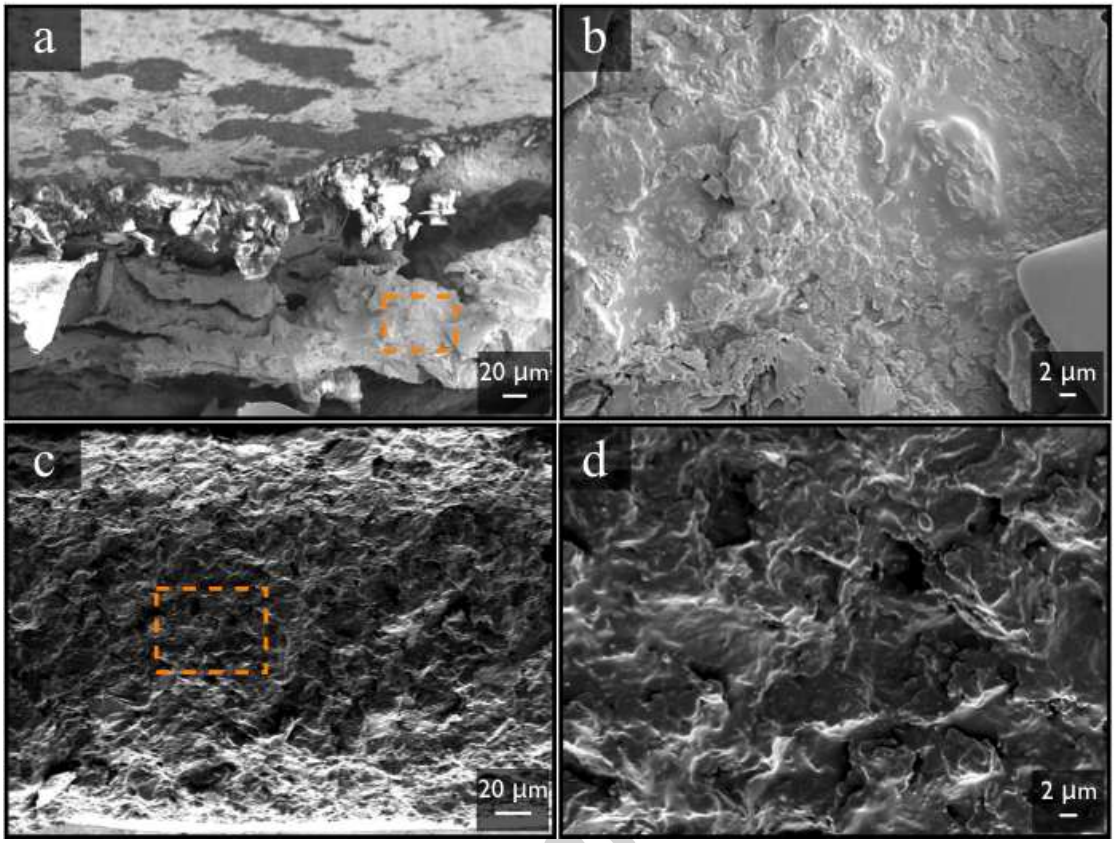

Fig. 6. SEM images of hybrid ECAs with 60 wt% Ag/0.75 wt% Gr(s): solvent-free formulation at low magnification (a) and at high magnification referenced from orange box (b); solvent-assisted formulation at low magnification (c) and at high magnification referenced from orange box (d).

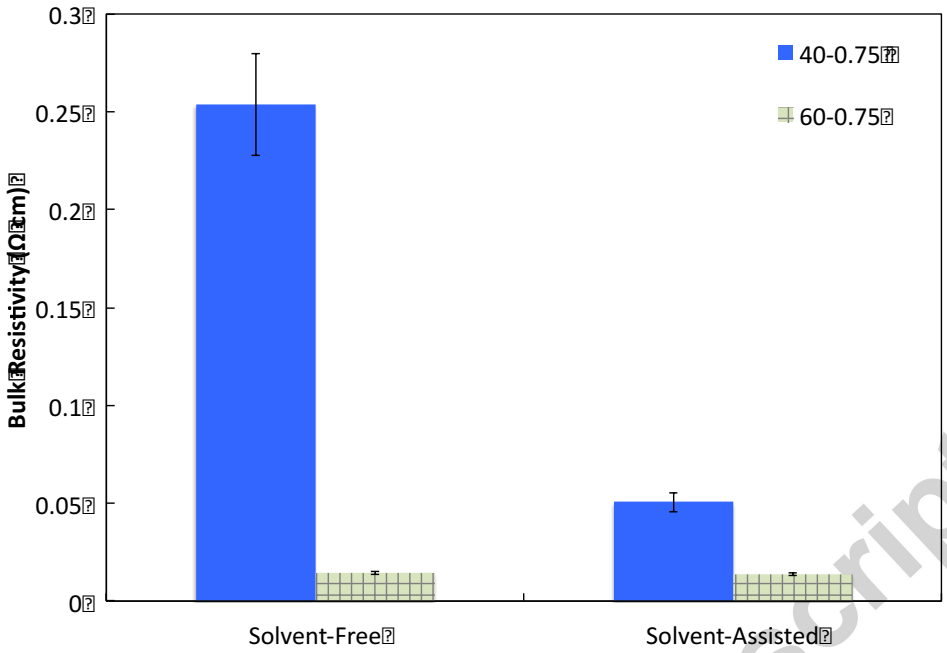

Fig. 7 Bulk resistivity comparison of solvent-assisted and solvent-free formulations with 40 wt% Ag/0.75 wt% Gr(s) and 60 wt% Ag/0.75 wt% Gr(s).